JACS
JOURNAL OF THE AMERICAN CHEMICAL SOCIETY
Article
pubs.acs.org/JACS

Thermally Active Hybridization Drives the Crystallization of DNA-Functionalized Nanoparticles

Ting I. N. G. Li, Rastko Sknepnek,‡ and Monica Olvera de la Cruz*

Department of Materials Science and Engineering, Northwestern University, Evanston, Illinois 60208, United States

Supporting Information

ABSTRACT: The selectivity of DNA recognition inspires an elegant protocol for designing versatile nanoparticle (NP) assemblies. We use molecular dynamics simulations to analyze dynamic aspects of the assembly process and identify ingredients that are key to a successful assembly of NP superlattices through DNA hybridization. A scale-accurate coarse-grained model faithfully captures the relevant contributions to the kinetics of the DNA hybridization process and is able to recover all experimentally reported to date binary superlattices (BCC, CsCl, AlB_2, Cr_3Si, and Cs_6C_{60}). We study the assembly mechanism in systems with up to 10^6 degrees of freedom and find that the crystallization process is accompanied with a slight decrease of enthalpy. Furthermore, we find that the optimal range of the DNA linker interaction strengths for a successful assembly is $12-16k_BT$, and the optimal mean lifetime of a DNA hybridization event is $10^{-4}-10^{-3}$ of the total time it takes to form a crystal. We also obtain the optimal percentage of hybridized DNA pairs for different binary systems. On the basis of these results, we propose suitable linker sequences for future nanomaterials design.

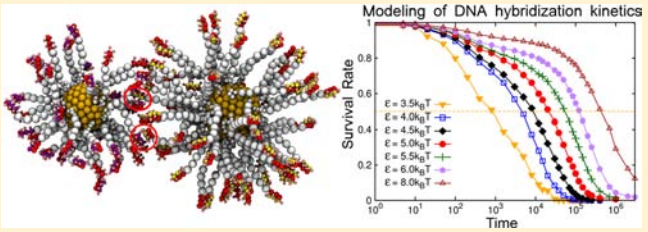

INTRODUCTION

Addressing the challenges of designing and synthesizing arbitrary assemblies by controlling properties of nanoscale building blocks has been a focus of both fundamental science[1−3] and practical applications.[4−7] Compared to common atomistic assemblies (Ångström length scale), nanoscale building blocks (size range ∼1−100 nm) are larger by over 2 orders of magnitude; thus, their assemblies possess unique electronic, optical, mechanical, and magnetic properties.[7,8] They offer potential applications in medical diagnostics (programmable recognition),[4,9] catalysis,[10] and energy conversion and as plasmonic nanomaterials.[6] An elegant method for designing building blocks involves coating individual nanoparticles (NPs) with DNA and using DNA recognition to selectively link NPs to form complex assemblies, as proposed in the mid-1990s.[11,12] Achieving this goal in a controlled setting is challenging, and it took over a decade for experiments to transition from the era of random NP aggregates[11−16] to the one of basic NP superlattices (e.g., those with face-centered cubic and body-centered cubic symmetries).[17,18] The past 5 years have been particularly prolific with great advances being made in the successful synthesis of one-, two-, and three-dimensional NP assemblies.[17,19,20] Modeling of the NP assembly process was developed concomitantly at a similar pace.

NP assemblies can easily become kinetically trapped in an amorphous state, a seemingly unavoidable predicament for both experiments and simulations in the early days. This challenge was overcome by carefully selecting the "sticky" DNA linker (i.e., the terminal single-stranded portion designed to hybridize with its complementary strand). Specifically, experimentalists shortened the linker sequence from 12 bases[11,13] to 6 bases (-TTCCTT for complementary linkers[19]) and 4 bases (-CGCG in self-complementary cases[17,20,21]) to provide a high rate of attachment and detachment hybridization events as argued by Macfarlane et al.[21] The same study also proposed a design rule that "the structure with maximum number of hybridizations will be thermodynamically favorable".[19] A number of serious concerns have been raised about the DNA hybridization kinetics, DNA behavior during the assembly process, and the amount of hybridizations (i.e., hybridized DNA pairs) in different assemblies.[19,22,23] However, current experimental techniques cannot reach a sufficient resolution to probe an individual hybridization event. Nevertheless, a quantitative understanding of the physical processes responsible for a successful hybridization event is essential for the control and the design of DNA-programmed materials.[24−26]

To address these issues via simulations, a primary obstacle is the lack of a reliable, detailed dynamic modeling approach. Several theoretical studies of disordered gels have been reported,[27−29] as well as a substantial number of analytical and numerical models for systems confined to a lattice.[19,30−32] Nonetheless, only a few have been able to successfully capture crystallization from random initial states involving explicit DNA chains with experimentally relevant interaction parameters.[33] To address these concerns, we applied a robust modeling approach[33,34] (Figure 1) to investigate the crucial ingredients

Received: January 3, 2013
Published: May 12, 2013

   dx.doi.org/10.1021/ja312644h | J. Am. Chem. Soc. 2013, 135, 8535−8541

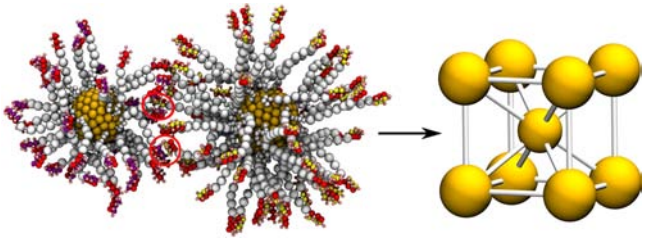

Figure 1. Schematic representation of DNA-guided NP assembly. Two building blocks used in simulations are shown on the left. DNA hybridization events are circled in red.

for successful DNA-programmed crystallization, namely, the linker strength suitable for assembling distinct superlattices, the hybridization kinetics that is key to superlattice formation, and the corresponding percentage of hybridizations.

In a recent study,[34] we employed an elegant coarse-grained model developed by Knorowski et al.[33] to map the experimental phase diagram of binary mixtures of DNA-coated NPs obtained by the Mirkin group.[19] Here we use the same model to identify the main ingredients for a successful crystallization, and to address the important question of the self-assembly dynamics previously not analyzed. We provide a quantitative analysis of DNA-guided NP assembly as a function of the properties of the sticky ends of the DNA. We show that the thermally active hybridization (i.e., a DNA hybridization process in which bonds between complementary DNA bases form and break as a result of thermal fluctuations) is the key to achieving successful crystallization. Furthermore, we provide an outline for the general selection of suitable linker sequences and analyze the hypothesized assembly mechanism at the level of a single DNA chain. Our study can provide basic guidelines for future nanomaterials design that go beyond current experiments, which typically employ only one or two building block species and at most two types of sticky-end interactions.

MODEL OF THERMALLY ACTIVE HYBRIDIZATION

In order to capture as accurately as possible the sizes and stiffnesses for different parts of DNA chains, we use the flanking bead model of Knorowski et al.[33] Beads for the double-stranded DNA (dsDNA) segments have diameters of ≈2 nm (representing ≈5 dsDNA base pairs), comparable to the diameter of an actual dsDNA chain, while beads for single-stranded (ssDNA) regions are sized at ≈1 nm (representing 2−3 ssDNA bases). We point out that due to the coarse-grained nature of the model, the direct comparison of the bead size to the actual DNA chain is very hard and should only be considered as an approximate estimate. For example, this model has no resolution to capture the subtle shrinking of base-pair spacing as a result of hybridization.[35] However, we believe that such effects do not significantly affect mesoscale properties and that this model can accurately capture key aspects of the assembly process. In order to mimic the experimentally reported values, the persistence length of dsDNA is set to ≈50 nm by applying an angle potential along the dsDNA chain:

$$V_{\text{angle}}(\theta) = \frac{1}{2}k_\theta(\theta - \pi)^2 \quad (1)$$

where θ is the angle between two bonds meeting at a bead and $k_\theta \approx 20k_BT$. For computational feasibility, the nonbonded interaction between any pair of beads is modeled with the Lennard-Jones potential. The details of the model and the simulation protocol are presented in ref 34. Molecular dynamics (MD) simulations were performed on Graphics Processing Units (GPUs) with the HOOMD-Blue package[36−38] under the constant number of particles, volume, and temperature (NVT) ensemble, with the temperature controlled via a Nosé-Hoover thermostat.[39,40] Periodic boundary conditions were applied to all simulated systems and each simulation started from an independent random initial configuration.

To simulate the formation of NP superlattices, it is essential to retain a high level of hybridization events, i.e., the hybridization must be highly dynamic. As opposed to passive hybridization where bonds are unlikely to dissociate, active hybridization can bring down the energy barrier between a kinetically trapped structure and a state in thermodynamic equilibrium, opening a pathway to a successful crystallization. Therefore, the essential part of this coarse-grained model is the proper parametrization of the force field for the complementary sticky ends.

We achieve a thermally active hybridization by carefully tuning the bond strength (ε) and the interactive range (σ) between the coarse-grained beads of the sticky ends. $\varepsilon \approx 4.5k_BT$ and $\sigma \approx 1.2$ nm serve as suitable values that enable crystallization while achieving a fully active hybridization. We note that these parameters are very close to the experimental estimates for the DNA base pair interaction: ref 22 reports a distance of 1.2 nm between the hybridized 7-base pair sticky ends; for the value of ε, we will provide a detailed comparison with experiments in the section Optimal Linker Strength for Various Binary Systems.

In order to rationalize the model, in Figure 2 we plot two quantities central for quantifying the hybridization process. The top plot presents the survival rate of a set of hybridizations as a function of the simulation time as a direct way to quantify the dynamics. At time $t = 0$ we record all pairs of sticky ends that are hybridized and track those pairs as the system evolves in time. Correspondingly, the fraction of hybridizations, f_H, that survive up to a time t decreases below 1. We

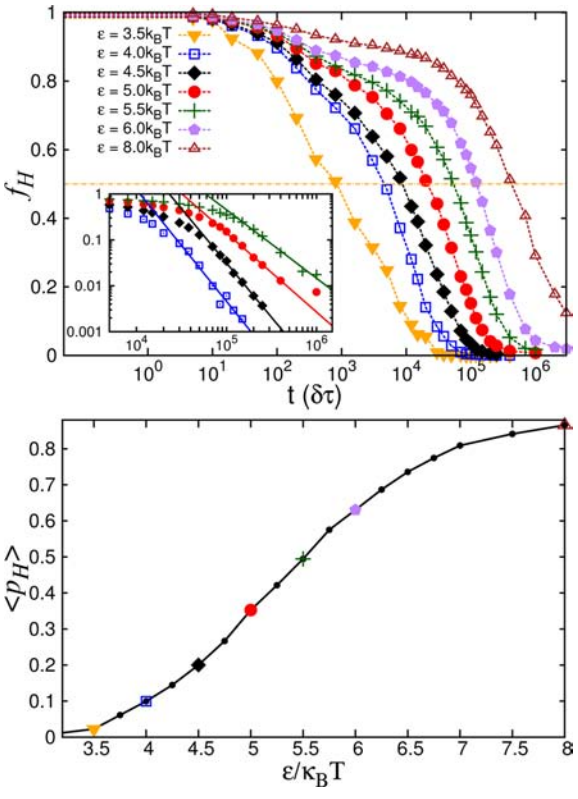

Figure 2. Top: Fraction of hybridizations f_H that survive up to a time t. Inset: A power-law fit of the long-time tail of $f_H \propto t^{-b}$. The exponents are between $b \approx 2.4$ (for $\varepsilon = 4k_BT$) and $b \approx 1.5$ (for $\varepsilon = 5.5k_BT$), which are in good agreement with ref 41. Bottom: Percentage of hybridizations $\langle p_H \rangle$ (relative to the maximum number of hybridizations in this system) vs ε. The same type of symbols represent the same ε in both plots. ε is measured in units of k_BT. Error bars are smaller than the symbol size.

dx.doi.org/10.1021/ja312644h | J. Am. Chem. Soc. 2013, 135, 8535−8541

note that t, measured in units of $\delta\tau = (m\sigma^2/\varepsilon)^{1/2}$, with m being the unit bead mass, is represented on a logarithmic scale, and that the mean lifetime of a hybridization (time at which $f_H = 0.5$) is very sensitive to the interaction strength and can change by orders of magnitude if ε is slightly varied. We fit the tail of the f_H curve to a power law $f_H(t) \sim t^{-b}$ as suggested by Biancaniello et al.,[41] and obtain powers $b \approx 1.5-2.4$ in agreement with ref 41 (see the inset in upper panel of Figure 2). The bottom plot in Figure 2 shows the percentage of hybridizations $\langle p_H \rangle$ relative to the maximum number of possible sticky-end pairs in the system as a function of ε. Clearly, larger bond strength leads to a larger percentage of hybridizations.

As the selection of the linker strength is crucial for NP superlattice design, we propose two guidelines here. First, *sufficient hybridizations*, where by "sufficient" it is meant that the percentage of hybridized sticky ends in equilibrium has to be considerable (precise quantification of this statement will be given below), otherwise DNA interactions are inadequate to compete with the thermal fluctuations of the NPs and therefore would fail to successfully guide the assembly. We use the percentage of hybridizations $\langle p_H \rangle$ instead of the number of hybridizations per particle as the former only depends on ε and the latter varies with different sizes of NPs. Second, *thermally active hybridization*, meaning that linkers should be able to easily attach to and detach from their complementary counterparts as a result of thermal fluctuations, thus allowing an easy escape from any kinetically trapped structure. However, small ε favors the dynamics (i.e., it favors hybridizations with shorter lifetimes) but leads to a low total number of hybridizations, while large ε brings more hybridizations but inhibits their dynamics. Therefore there is only a narrow range of values of ε for which these two competing effects balance to allow successful assembly. In the following, we identify the suitable range of ε for various lattices.

RESULTS AND DISCUSSION

Multi-Scale Simulation Systems To Study Assembly Mechanism. The scale-accurate coarse-grained model has been extensively tested for robustness and reliability. It enables us to study the assembly of various superlattices,[19] ranging from BCC and CsCl to more complicated symmetries:[34] AlB_2 (anisotropic unit cell), Cr_3Si (8 building blocks per cubic unit cell), and Cs_6C_{60} (the newly simulated structure first reported in this paper). Bearing a smaller hydrodynamic size ratio of two building block species, generally found to be ~0.3−0.4,[19] the Cs_6C_{60} lattice is more difficult to equilibrate than the other structures. Accordingly, we employed an annealing process to accelerate the formation of the Cs_6C_{60} crystal, although similar annealing was not required for the other lattices (for details, see Figure S2 in the Supporting Information). To date, we have successfully recovered all experimentally reported binary NP superlattices. The ability of a simple coarse-grained model to successfully reproduce a wide array of experimentally observed crystalline superlattices strongly supports the notion that the assembly process is universal and is not sensitive to details of the system's chemistry.

We performed MD simulations to study the assembly mechanism. In ref 34, systems with ~30−60 building blocks form crystals within $\sim 3 \times 10^7$ simulation time steps. In this study, we have expanded the system sizes to ~100−250 building blocks (Figure 3). These larger systems require $\sim 4 \times 10^8$ steps to successfully crystallize, corresponding to weeks or even months of GPU time per single run. We have also reexamined numerous points in the previously reported phase diagram[34] with these larger systems: CsCl lattices with $4 \times 4 \times 4$ unit cells (128 building blocks) and $5 \times 5 \times 5$ unit cells (250 building blocks), and AlB_2 lattices with $4 \times 3 \times 3$ unit cells (108 building blocks). A comparison of the different system sizes is summarized in Table 1 and Figure 4. In general, the simulation time for the entire assembly process increases by 5−10 times when shifting from systems with ~50 building blocks to systems with ≳100 building blocks. However, there is no corresponding increase in the number of time steps required to transition from an average value p_H in the disordered state to the value characteristic of the ordered structure. Hence, in Figure 4 we observe a sharp jump in p_H for larger systems, contrary to the moderate p_H increase in smaller systems. This can be simply understood as follows: it takes longer for a larger system to rearrange NPs in order to initiate the crystallization process, while the time required to form a crystal once all NPs are in place is independent of the system size (note that periodic boundary conditions are always applied).

For each simulated superlattice, we observed a noticeable decrease of the potential energy occurring simultaneously with the increase in p_H. Each hybridization of two complementary linkers decreases the potential energy by 3ε (each sticky end is represented by three beads in the simulation) and is thus energetically favorable. As expected, the overall potential energy decrease ΔU is found to be approximately equivalent to $3\varepsilon\Delta p_H N$, with N being the maximum number of hybridizations and Δp_H is the change in p_H. We point out that this increase of

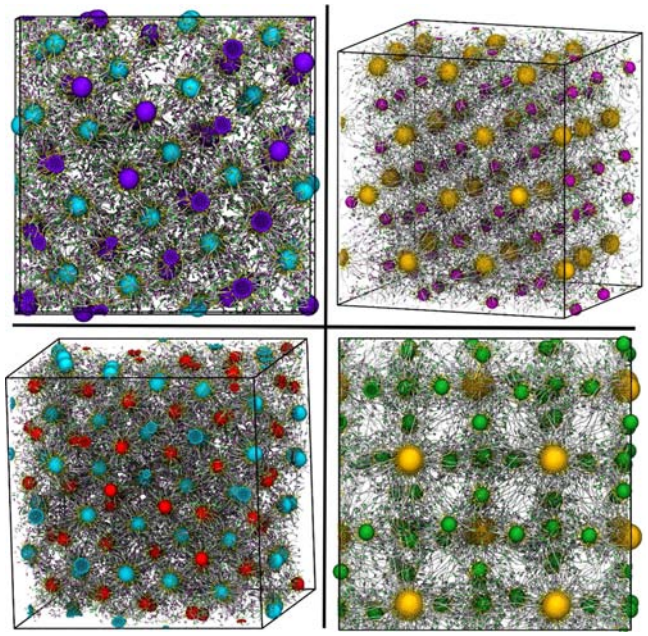

Figure 3. Binary systems with ~100−250 building blocks (see assembly movies in Supporting Information). Top-left: BCC (128 building blocks). Top-right: AlB_2 (108 building blocks). Bottom-left: CsCl (250 building blocks). Bottom-right: Cs_6C_{60} (112 building blocks). All snapshots were generated with the Visual Molecular Dynamics (VMD) package[42] and rendered with Tachyon ray-tracer.[43]

Table 1. Comparison of the Number of Simulation Time Steps Required for the Equilibrium Structures To Form as Well as for the Average Number of Hybridizations To Equilibrate for Systems with Different Numbers of Building Blocks

building blocks	time step[a]	steps for self-assembly	steps for p_H to equilibrate
~50	0.0025	$\sim(2-3) \times 10^7$	$\sim(2-3) \times 10^7$
≳100	0.0015	$\sim(2-4) \times 10^8$	$\sim(3-4) \times 10^7$

[a]The timestep $\delta\tau$ is measured in units of $\sqrt{(m\sigma^2/\varepsilon)}$.

dx.doi.org/10.1021/ja312644h | J. Am. Chem. Soc. 2013, 135, 8535−8541

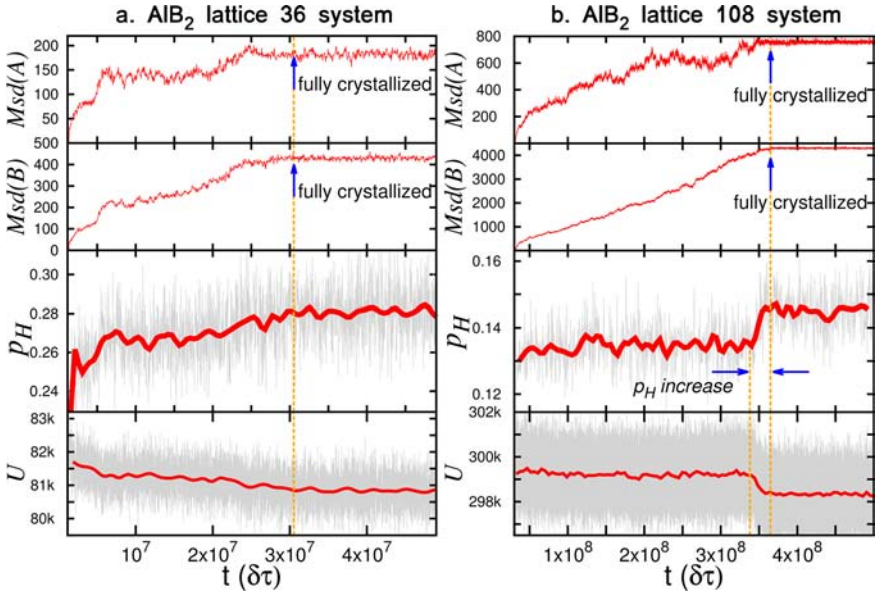

Figure 4. Comparison of the crystallization process between two representative system sizes (a) AlB_2 lattice with 36 building blocks ($3 \times 2 \times 2$ unit cells) in the simulation box and (b) AlB_2 lattice with 108 building blocks ($4 \times 3 \times 3$ unit cells) in the simulation box. The x-axis plots the simulation time step. Top two rows: Mean square displacement, $\mathrm{Msd}(\alpha)$ ($\langle \Delta r_\alpha^2(t) = \langle (\vec{r}_\alpha(t) - \vec{r}(0))^2 \rangle$, α = (A,B) is the building block species). Middle bottom: The percentage of hybridizations (p_H). Bottom: total potential energy U of the system. The arrows indicate that the crystallization process has been completed. For time beyond the dashed line, the system is crystalline.

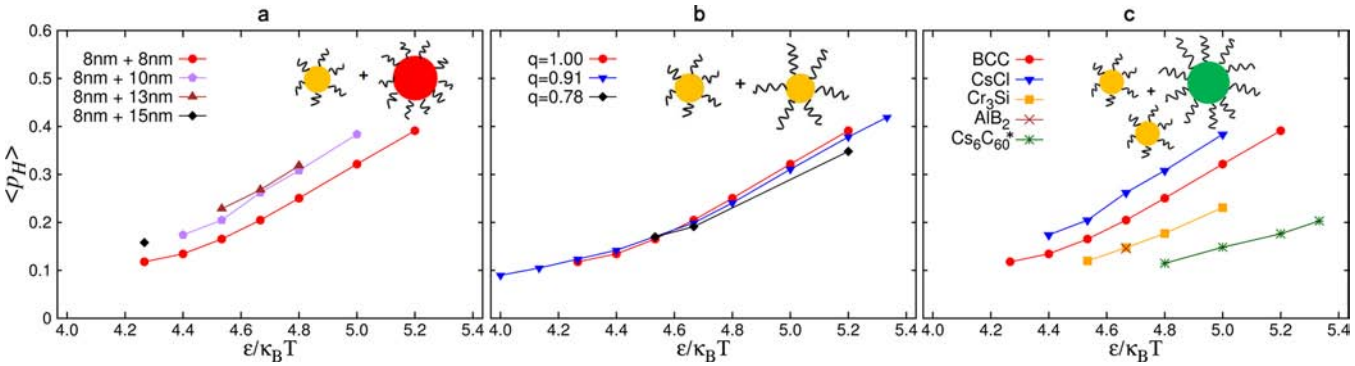

Figure 5. Optimal linker strength and corresponding $\langle p_H \rangle$ for various binary systems. Studied parameters are (a) DNA coverage ratio r (i.e., ratios of the sizes of two NP cores), (b) size ratio q (DNA length), and (c) lattice type. Note that Cs_6C_{60} is the only system for which an annealing process was used. Error bars are smaller than the symbol size.

p_H is only ~1−2%, which is much smaller than naively expected and may easily be masked by thermal fluctuation. We also emphasize that in a recent study of Knorowski and Travesset[2] a similar decrease of the potential energy was not observed. We will discuss this discrepancy in more detail below.

In addition, we examined the stability of the self-assembled structures in a quasi-infinite (open boundary) simulation box (see online movies of stability tests in Supporting Information). As expected, crystallized clusters are more stable (melt at higher temperature) than their amorphous counterparts, and larger crystals are more stable than smaller ones. The smallest stable crystal is found to involve ~200 building blocks (see Table S3 in the Supporting Information).

Optimal Linker Strength for Various Binary Systems. As it can be seen from the proposed guidelines for the linker sequence design, crystals only form over a finite range of the interaction strength, ε. Width of this range quantifies the sensitivity (or ease) with which one might expect crystallization to occur in experiments. Similarly, a detailed knowledge of the range of optimal linker strengths $\Delta\varepsilon$ and the corresponding average hybridization percentage $\langle p_H \rangle$ as a function of various design parameters would be extremely valuable to guide experiments.

In this section, we study (i) various binary systems with BCC, CsCl, AlB_2, Cr_3Si, and Cs_6C_{60} symmetries, and (ii) three design parameters, including DNA coverage (the number of DNA chains per particle) ratio (r), hydrodynamic size ratio (q), and stoichiometry (lattice type), as reported in the experimental phase diagrams.[19,34] As a reference, the small building blocks (type A) are kept the same for all designs: an 8 nm NP core covered with 40 DNA chains of length 14 nm (five coarse-grained beads in the dsDNA segment). All values of $\langle p_H \rangle$ in this section are calculated with respect to A. In Figure 5 we show $\langle p_H \rangle$ as a function of the three design parameters, r, q, and the lattice stoichiometry. Outside the region of the optimal linker strength, the system is either kinetically trapped in an amorphous state or remains liquid, in agreement with experiments.

Regarding the DNA coverage ratio, r, we find that larger coverage ratio leads to larger $\langle p_H \rangle$ *until saturated*. For efficiency,

dx.doi.org/10.1021/ja312644h | J. Am. Chem. Soc. 2013, 135, 8535−8541

here we focus on a system with CsCl symmetry with 4 × 4 × 4 unit cells. Lengths of all DNA chains are kept equal at 14 nm, while only the DNA coverage of the large building blocks B is varied with the NP core size. Details of the four studied DNA coverages are given in Table S2. Note that each data point in Figure 5 represents the result of an independent simulation that successfully self-assembled into superlattices within ∼5 × 10^8 steps. As expected, larger coverage ratios lead to more complementary DNA chains, and thus enhance the $\langle p_H \rangle$. However, the $\langle p_H \rangle$ will saturate as the coverage ratio goes beyond ∼2.0. Corresponding packing densities for each simulation data point are summarized in Table S4. These packing densities indicate a slight expansion of the lattice parameter with increasing linker strength. In addition, our results suggest that a coverage ratio closer to the inverse of the stoichiometry thus providing equal amounts of complementary linkers results in larger $\Delta\varepsilon$.

Regarding the size ratio, q, we find that $\Delta\varepsilon$ instead of $\langle p_H \rangle$ is significantly influenced by the size ratio. The same system as the one discussed above was simulated to study the effects of the size ratio, or specifically, the length of DNA chains. In this study, all of the NP cores are identical with an 8 nm diameter. Since the A's are fixed, the size ratio of the two building blocks varies as a result of the different lengths of the DNA chains for the type B building blocks. The designs of the four size ratios included in this study range from 0.6 to 1.0. From the results shown in Figure 5b, the length of the DNA chains has a limited ability to significantly shift the $\langle p_H \rangle$. Oppositely, $\Delta\varepsilon$ is greatly affected by q: for CsCl systems, q = 0.91 exhibits the broadest range of $\Delta\varepsilon$ among the four designs, while for the system with q = 0.6 it is relatively difficult to form any superlattice within 5 × 10^8 steps.

Finally, regarding the lattice type, we find that a superlattice with higher symmetry has a broader $\Delta\varepsilon$. Here, we explore to what extent lattice type can influence $\Delta\varepsilon$ and $\langle p_H \rangle$. We select one representative design roughly from the center of the reported phase diagrams[19,34] for each of the lattices BCC (128 building blocks), CsCl (128 building blocks), Cr_3Si (64 building blocks), AlB_2 (108 building blocks), and Cs_6C_{60} (112 building blocks). Therefore, in this set of designs, either stoichiometry or the DNA coverage ratio or the size ratio can vary. Note that all of the simulations were performed at a constant temperature except for the Cs_6C_{60} system, which included annealing for reasons discussed earlier. The simulation results suggest that the range of linker strengths narrows down from BCC to CsCl to Cr_3Si to AlB_2. This order is consistent with the order of superlattice symmetry: the Cr_3Si lattice has more building blocks per unit cell than BCC or CsCl, while AlB_2 is the only noncubic lattice of these.

We relate larger values of $\Delta\varepsilon$ to easier crystallization. Therefore, consistent with experiments,[17] a design of higher symmetry with DNA coverage ratio close to the inverse of the stoichiometry is easier to self-assemble due to a broader range of optimal sticky end strengths. As for the simplest binary building block structure, i.e., BCC structure, a size ratio of ∼0.9 instead of 1.0 should be most suitable to crystallize.

Regarding the linker strength, we directly compare our predictions with experiments. For binary systems, the predicted value for the suitable bond strength per bead should fall into the range of ∼4.0−5.4k_BT. We note that since each linker is represented by three coarse-grained beads, we suggest that the linker strength should be ∼12−16k_BT, or ∼29−40 kJ/mol at room temperature.[44] This range fits well with the experimentally reported linker sequences, as summarized in Table 2. Experiments confirm that it takes a much longer time to assemble a superlattice for larger linker strengths, which also poses a difficulty for MD simulations with large ε. Nevertheless, the excellent quantitative agreement between the optimal linker strength obtained from the coarse-grained model and the experimentally reported values goes beyond expectation of the quantitative predictive power of the relatively simple coarse-graining scheme used in this study. Based on the obtained optimal linker strength ε, we refer to Figure 2 to quantify its corresponding thermodynamic properties. We conclude that the mean lifetime of desired hybridizations should range from 10^{-4} to 10^{-3} of the total time it takes p_H to reach its ordered-state value, as this increase (but not the entire assembly time) is independent of the system size.

Table 2. Linker Strength for Sequences Used in Experiments

sequence	ΔG (kJ/mol)[44]
GCGC[17,20]	41.0
TTCCTT[19]	42.3
TTTCCTT[17]	50.2

As expected, the range of optimal linker strengths to guide superlattice assembly is not too broad, and typically a 4- to 8-base linker is sufficient. The corresponding lifetime of these hybridizations can vary by one to two orders of magnitude. Nevertheless, there are still numerous—hundreds to thousands—possible selections of DNA pairs that fit into this range, within which tens of sequences are self-complementary, thus providing a rich toolkit for controllable material design.

SUMMARY AND CONCLUSIONS

In this study we have shown that a scale-accurate coarse-grained model faithfully captures the relevant DNA-pair interaction. Successful modeling of the thermally active DNA hybridization events enables us to efficiently simulate the assembly process. The model is robust and reproduces all of the experimentally reported binary superlattices, including BCC, CsCl, AlB_2, Cr_3Si, and Cs_6C_{60} lattices, over a wide range of system sizes with 50−250 building blocks. We note that the system sizes studied in this paper, although small, exceed the size of a critical nucleus. Knorowski et al.[2] recently reported that the critical nucleus contains ∼40 building blocks, and we also showed that the 200 building block crystal remains stable upon removing the periodic boundaries. By analyzing the dynamics of the assembly process we observed that the increase of the percentage of hybridizations (p_H) to the value characteristic to the crystalline state is independent of the system size. We argued that the superlattice assembly is not sensitive to the details of the chemistry of DNA chains, but is far more general and only dependent on the active nature of the hybridization events between soft overlapping DNA coats of neighboring NPs.

In this study we observed an increase in p_H accompanied by a sharp decrease in the total potential energy during the crystallization. Such a drop of the potential energy suggests that enthalpy plays a significant role in the crystal formation process. However, this observation is inconsistent with findings of Knorwski and Travesset,[2] who did not observe a similar drop of the potential energy accompanying crystallization, thus indicating that the crystallization is entirely entropy driven. We speculate that this discrepancy is in part due to the different overall DNA coverage of NP cores in two studies. In our case

dx.doi.org/10.1021/ja312644h | J. Am. Chem. Soc. 2013, 135, 8535−8541

the DNA coverage is significantly denser (~3 times) and once the particles are in place, the system can further lower its free energy by forming additional hybridization between nearby DNA strands. We note that a full account of the relative importance of enthalpy vs entropy in the assembly process would require a careful analysis of the free energy of the assembly process, which is a daunting task for the present model well beyond the scope of this study.

We proposed two guidelines to remedy the linker strength trade-off: (i) *sufficient number of hybridizations* and (ii) *thermally active hybridization*. We have discussed the optimal linker strength, hybridization kinetics, and $\langle p_H \rangle$ for various systems. While this work is based on the dsDNA-coated NP (size ~10 nm) systems from the Mirkin group, we point out that the suitable linker strength may shift to a larger value for heavier colloidal systems or more flexible ssDNA systems. We envision a simple prescription for future nanomaterials design with versatile DNA interactions.

Finally, we briefly discuss the ability of the coarse-grained model to predict actual experiments. Due to the coarse-grained nature of the model used in this study it is nontrivial to make connections to the experiments and discern which predictions are quantitative and which are only qualitative. As the degree of departure of the parameters of a real system grows with the level of coarse-graining, it requires a lot of tuning (and trial and error attempts) to construct a coarse-grained model that is simple enough to be efficiently simulated but at the same time detailed enough to capture relevant processes. While adopting the model of Knorowski and Travesset[2] to the experimental systems studied in the Mirkin group, we paid particular attention to retain the relative sizes as faithful as possible to the actual system. The used linker strengths are of the same order of magnitude as those in real DNA molecules, thus suggesting that it would be reasonable to expect that, e.g., the observed DNA kinetics should also be comparable to the experiments. While clearly this model cannot capture all aspects of the assembly in this complex nanocomposite material, to the best of our knowledge this is to date the most detailed model that is able to capture crystallization process of many NPs.

■ ASSOCIATED CONTENT

Supporting Information

Force field of the model, system packing densities, simulation of Cs_6C_{60} superlattice, and critical crystal size. Simulation movies of the assembly process and crystal stability test: si_002.mpg = AlB_2 108 system formation; si_0003.mpg = AlB_2 108 system rock; si_004.mpg = CsCl 250 system formation; si_005.mpg = CsCl 54 system stability test; si_006.mpg = CsCl 250 system stability test. This material is available free of charge via the Internet at http://pubs.acs.org.

■ AUTHOR INFORMATION

Corresponding Author

m-olvera@northwestern.edu

Present Address

‡R.S.: Department of Physics, Syracuse University, Syracuse, NY 13244

Notes

The authors declare no competing financial interest.

■ ACKNOWLEDGMENTS

We are grateful to Christopher Knorowski and Alex Travesset for numerous illuminating discussions and for sharing their scripts with us. We thank Youngeun Kim, Rob Macfarlane, Chad Mirkin, and Ryan Thaner for discussions about the details of the experiments. We also thank Chloe Funkhouser, Kevin Kohlstedt, and Xiaohan Zeng for critical reading of the manuscript and helpful discussions. T.L. gratefully acknowledges support from the Ryan Fellowship and the Northwestern University International Institute for Nanotechnology. This work is funded by AFOSR MURI FA9550-11-1-0275 at the International Institute for Nanotechnology at Northwestern University. The computational work was performed using TARDIS computer cluster supported by NSSEFF FA9550-10-1-0167.

■ REFERENCES

(1) Wang, Y.; Wang, Y.; Breed, D. R.; Manoharan, V. N.; Feng, L.; Hollingsworth, A. D.; Weck, M.; Pine, D. J. *Nature* **2012**, *491*, 51−55.
(2) Knorowski, C.; Travesset, A. *Soft Matter* **2012**, *8*, 12053−12059.
(3) Dai, W.; Kumar, S. K.; Starr, F. W. *Soft Matter* **2010**, *6*, 6130−6135.
(4) Mirkin, C. A. *MRS Bull.* **2010**, *35*, 532−539.
(5) Carter, J. D.; LaBean, T. H. *ACS Nano* **2011**, *5*, 2200−2205.
(6) Sebba, D. S.; Mock, J. J.; Smith, D. R.; LaBean, T. H.; Lazarides, A. A. *Nano Lett.* **2008**, *8*, 1803−1808.
(7) Daniel, M. C.; Astruc, D. *Chem. Rev.* **2004**, *104*, 293−346.
(8) Shevchenko, E. V.; Talapin, D. V.; Kotov, N. A.; O'Brien, S.; Murray, C. B. *Nature* **2006**, *439*, 55−59.
(9) Cutler, J. I.; Auyeung, E.; Mirkin, C. A. *J. Am. Chem. Soc.* **2012**, *134*, 1376−1391.
(10) Lin, L.; Liu, Y.; Tang, L.; Li, J. *Analyst* **2011**, *136*, 4732−4737.
(11) Mirkin, C. A.; Letsinger, R. L.; Mucic, R. C.; Storhoff, J. J. *Nature* **1996**, *382*, 607−609.
(12) Alivisatos, A. P.; Johnsson, K. P.; Peng, X.; Wilson, T. E.; Loweth, C. J.; Bruchez, M. P.; Schultz, P. G. *Nature* **1996**, *382*, 609−611.
(13) Storhoff, J. J.; Lazarides, A. A.; Mucic, R. C.; Mirkin, C. A.; Letsinger, R. L.; Schatz, G. C. *J. Am. Chem. Soc.* **2000**, *122*, 4640−4650.
(14) Valignat, M. P.; Theodoly, O.; Crocker, J. C.; Russel, W. B.; Chaikin, P. M. *Proc. Natl. Acad. Sci. U.S.A.* **2005**, *102*, 4225−4229.
(15) Jin, R.; Wu, G.; Li, Z.; Mirkin, C. A.; Schatz, G. C. *J. Am. Chem. Soc.* **2003**, *125*, 1643−1654.
(16) Mucic, R. C.; Storhoff, J. J.; Mirkin, C. A.; Letsinger, R. L. *J. Am. Chem. Soc.* **1998**, *120*, 12674−12675.
(17) Park, S. Y.; Lytton-Jean, A. K. R.; Lee, B.; Weigand, S.; Schatz, G. C.; Mirkin, C. A. *Nature* **2008**, *451*, 553−556.
(18) Nykypanchuk, D.; Maye, M. M.; van der Lelie, D.; Gang, O. *Nature* **2008**, *451*, 549−552.
(19) Macfarlane, R. J.; Lee, B.; Jones, M. R.; Harris, N.; Schatz, G. C.; Mirkin, C. A. *Science* **2011**, *334*, 204−208.
(20) Jones, M. R.; Macfarlane, R. J.; Lee, B.; Zhang, J.; Young, K. L.; Senesi, A. J.; Mirkin, C. A. *Nat. Mater.* **2010**, *9*, 913−917.
(21) Macfarlane, R. J.; Jones, M. R.; Senesi, A. J.; Young, K. L.; Lee, B.; Wu, J.; Mirkin, C. A. *Angew. Chem., Int. Ed.* **2010**, *49*, 4589−4592.
(22) Rogers, W. B.; Crocker, J. C. *Proc. Natl. Acad. Sci. U.S.A.* **2011**, *108*, 15687−15692.
(23) Sambriski, E. J.; Schwartz, D. C.; de Pablo, J. J. *Proc. Natl. Acad. Sci. U.S.A.* **2009**, *106*, 18125−18130.
(24) Guo, P.; Sknepnek, R.; Olvera de la Cruz, M. *J. Phys. Chem. C* **2011**, *115*, 6484−6490.
(25) Zwanikken, J. W.; Guo, P.; Mirkin, C. A.; Olvera de la Cruz, M. *J. Phys. Chem. C* **2011**, *115*, 16368−16373.
(26) Largo, J.; Starr, F. W.; Sciortino, F. *Langmuir* **2007**, *23*, 5896−5905.

(27) Sun, Y.; Harris, N. C.; Kiang, C. H. *Phys. A (Amsterdam, Neth.)* **2005**, *354*, 1−9.
(28) Park, S. Y.; Stroud, D. *Phys. Rev. B* **2003**, *68*, 224201.
(29) Lu, P. J.; Zaccarelli, E.; Ciulla, F.; Schofield, A. B.; Sciortino, F.; Weitz, D. A. *Nature* **2008**, *453*, 499−503.
(30) Mladek, B. M.; Fornleitner, J.; Martinez-Veracoechea, F. J.; Dawid, A.; Frenkel, D. *Phys. Rev. Lett.* **2012**, *108*, 268301.
(31) Lara, F. V.; Starr, F. W. *Soft Matter* **2011**, *7*, 2085−2093.
(32) Padovan-Merhar, O.; Lara, F. V.; Starr, F. W. *J. Chem. Phys.* **2011**, *134*, 244701.
(33) Knorowski, C.; Burleigh, S.; Travesset, A. *Phys. Rev. Lett.* **2011**, *106*, 215501.
(34) Li, T. I. N. G.; Sknepnek, R.; Macfarlane, R. J.; Mirkin, C. A.; Olvera de la Cruz, M. *Nano Lett.* **2012**, *12*, 2509−2514.
(35) Smith, S. B.; Cui, Y.; Bustamante, C. *Science* **1996**, *271*, 795−798.
(36) HOOMD-blue web page: http://codeblue.umich.edu/hoomd-blue.
(37) Anderson, J. A.; Lorenz, C. D.; Travesset, A. *J. Comput. Phys.* **2008**, *227*, 5342−5359.
(38) Nguyen, T. D.; Phillips, C. L.; Anderson, J. A.; Glotzer, S. C. *Comput. Phys. Commun.* **2011**, *182*, 2307−2313.
(39) Nosé, S. *Mol. Phys.* **1984**, *52*, 255−268.
(40) Hoover, W. G. *Phys. Rev. A* **1985**, *31*, 1695.
(41) Biancaniello, P. L.; Kim, A. J.; Crocker, J. C. *Phys. Rev. Lett.* **2005**, *94*, 58302.
(42) Humphrey, W.; Dalke, A.; Schulten, K. J. *Mol. Graphics* **1996**, *14*, 33−38.
(43) Stone, J. E. An Efficient Library for Parallel Ray Tracing and Animation. M.Sc. thesis, University of Missouri, Rolla, O, 1998.
(44) Breslauer, K. J.; Frank, R.; Blöcker, H.; Marky, L. A. *Proc. Natl. Acad. Sci. U.S.A.* **1986**, *83*, 3746−3750.